Strong Nonreciprocity in Modulated Resonator Chains through Synthetic Electric and Magnetic Fields

Christopher W. Peterson, Wladimir A. Benalcazar, Mao Lin, Taylor L. Hughes, and Gaurav Bahl

Phys. Rev. Lett. **123**, 063901 — Published 7 August 2019

DOI: 10.1103/PhysRevLett.123.063901

Strong nonreciprocity in modulated resonator chains through synthetic electric and magnetic fields

Christopher W. Peterson,[1] Wladimir A. Benalcazar,[2,3] Mao Lin,[2] Taylor L. Hughes,[2] and Gaurav Bahl[4]

[1] *Department of Electrical and Computer Engineering, University of Illinois at Urbana-Champaign, Urbana, IL, USA*
[2] *Department of Physics and Institute for Condensed Matter Theory, University of Illinois at Urbana-Champaign, Urbana, IL, USA*
[3] *Department of Physics, The Pennsylvania State University, University Park, PA, USA*
[4] *Department of Mechanical Science and Engineering, University of Illinois at Urbana-Champaign, Urbana, IL, USA*

(Dated: July 11, 2019)

We study nonreciprocity in spatiotemporally modulated 1D resonator chains from the perspective of equivalent 2D resonator arrays with a synthetic dimension and transverse synthetic electric and magnetic fields. The synthetic fields are respectively related to temporal and spatial modulation of the resonator chain, and we show that their combination can induce strong transmission nonreciprocity, i.e. complete isolation with only a weak perturbative modulation. This nonreciprocal effect is analogous to the Hall effect for charged particles. We experimentally implement chains of 2 and 3 spatiotemporally modulated resonators and measure over 58 dB of isolation contrast.

Reciprocity is a fundamental property of wave propagation in linear, time-reversal symmetric systems that implies invariance under a spatial inversion of inputs and outputs [1, 2]. Due to this constraint, reciprocal systems cannot provide important functions such as source protection [3] and directional signal routing [4], which are critical to many electromagnetic, optic, and acoustic applications. Reciprocity can be broken in linear systems biased with a vector quantity that is odd under time-reversal [5, 6] such as a magnetic field [4, 7]. However, because nonreciprocal devices that require magnetic fields are often difficult to integrate into larger systems, especially on-chip or in sensitive superconducting circuits, recent research has increasingly employed frequency-converting spatiotemporal modulation to break reciprocity through directional scattering [8–22] or amplification [23–25].

In this letter we study nonreciprocity in one-dimensional (1D) chains of coupled photonic resonators with spatiotemporally modulated resonance frequencies. We use a synthetic-dimension description of the modulated resonator chains, which can be interpreted as unmodulated 2D resonator arrays with a synthetic frequency dimension [26]. The synthetic dimension holds frequency-shifted copies of the original chain that are equivalent to the sidebands produced by modulation. This description is particularly useful because the frequency and phase of the modulation become equivalent to a "photonic gauge potential" with similar properties to the electromagnetic vector-potential that couples to charged particles [27–30]. This gauge potential can generate synthetic electric [31] and magnetic [15] fields for photons in the resonator array, enabling a rich variety of physical phenomena such as Bloch oscillations [31], topological insulators [29, 32, 33], and the Aharonov-Bohm effect [12, 13].

Reciprocity can be broken in synthetic arrays having a magnetic field, but doing so requires an additional mirror-symmetry breaking in the frequency dimension [29] since the synthetic magnetic field is always perpendicular to the plane of the array. Previous work has relied on additional elements such as filters [12, 13] or added loss [29] to break this symmetry. Here we introduce a new approach that uses a synthetic electric field to break mirror symmetry in the frequency dimension. When a synthetic magnetic field that breaks time-reversal symmetry is also present, the combination of the two synthetic fields breaks transmission reciprocity. A major advantage of this method is its simplicity: both synthetic fields are generated from the same reconfigurable modulation process, and the additional lossy elements required in previous work [12, 13, 29] are unnecessary. This effect is analogous to the Hall effect for charged particles, where perpendicular electric and magnetic fields induce a current in the $\vec{E} \times \vec{B}$ direction [34]. We show that this combination of synthetic fields can produce strong nonreciprocity, i.e., complete isolation with a weak perturbative modulation, when the both synthetic fields are tuned to maximize their respective symmetry-breaking. We experimentally verify this concept using short chains of coupled resonators implemented in microwave-frequency microstrip circuits, and observe greater than 58 dB (approximately six orders of magnitude) of isolation contrast.

As an illustrative case, we first consider a chain of two identical coupled resonators with intrinsic resonance frequencies ω_0, as illustrated in Fig. 1a. The coupling rate between the resonators is λ, and each resonator is also coupled to a port, forming a two-port coupled-cavity waveguide. The resonance frequency of the resonators is

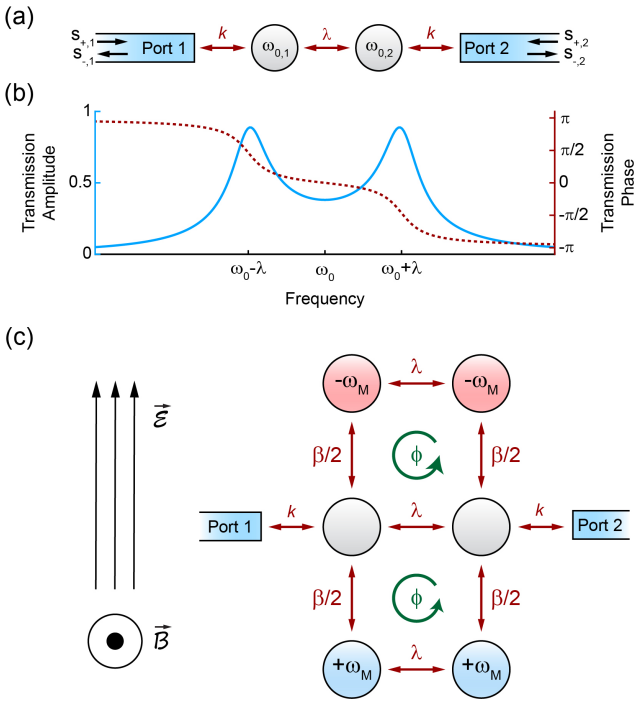

FIG. 1. (a) A chain of two coupled resonators coupled to two ports. The resonance frequencies $\omega_{0,n}$ are time-varying as described by Eq. (1). (b) Transmission, $\tau(\omega)$, for the chain of coupled resonators in the absence of modulation. Amplitude (solid blue) and phase (dashed red) are shown separately. The transmission phase is normalized to 0 at ω_0. (c) Pictorial representation of $\mathcal{H}$ using synthetic electric field $\vec{\mathcal{E}}$ and magnetic field $\vec{\mathcal{B}}$. The electric field generates a potential of $\mp\omega_M$ on the upper and lower chains respectively, and the magnetic field generates a direction-dependent phase shift of ϕ around each closed loop.

modulated sinusoidally with frequency ω_M according to

$$\begin{aligned}\omega_{0,1} &= \omega_0 + \beta\cos\left(\omega_M t\right)\\ \omega_{0,2} &= \omega_0 + \beta\cos\left(\omega_M t + \phi\right).\end{aligned} \tag{1}$$

The excitation amplitudes $a_{1,2}$ of resonators 1 and 2 (left and right circles in Fig. 1a, respectively) can be collected in a vector $|a(t)\rangle = \left[a_1(t), a_2(t)\right]^T$. Following Ref. 35, $|a(t)\rangle$ evolves in time according to

$$\frac{\partial}{\partial t}|a(t)\rangle = \left(i\Omega_0 + i\Omega_1(t) - \Gamma\right)|a(t)\rangle + iK^T|s_+(t)\rangle\,, \tag{2}$$

where the system parameters are written as the matrices

$$\Omega_0 = \begin{pmatrix}\omega_0 & \lambda\\ \lambda & \omega_0\end{pmatrix},\ \Gamma = \begin{pmatrix}\gamma & 0\\ 0 & \gamma\end{pmatrix},\ K = \begin{pmatrix}k & 0\\ 0 & k\end{pmatrix},$$

$$\Omega_1(t) = \begin{pmatrix}\beta\cos(\omega_M t) & 0\\ 0 & \beta\cos(\omega_M t + \phi)\end{pmatrix},$$

and $|s_+(t)\rangle, |s_-(t)\rangle$ are vectors that respectively correspond to the input and output amplitudes at the ports. The coupling between the ports and resonators is described by the coupling matrix K (k is the coupling constant between a resonator and a port). The total decay rates of the resonators are described by the matrix Γ (γ is the decay rate of each resonator), which satisfies $2\Gamma = K^\dagger K + \kappa$ [35]. The $K^\dagger K$ term accounts for the fields decaying into the ports, while the diagonal matrix κ accounts for any resistive or radiative losses in each resonator. The output of the system can be written as

$$|s_-(t)\rangle = |s_+(t)\rangle + iK|a(t)\rangle\,. \tag{3}$$

Since the system is periodic in time with frequency ω_M, it is convenient to work in the frequency domain. Using the Fourier transform $|a(\omega)\rangle = \int dt\,|a(t)\rangle\,e^{-i\omega t}$, in steady-state Eq. (2) becomes

$$\begin{aligned}\omega|a(\omega)\rangle = H_0|a(\omega)\rangle + K^T|s_+(\omega)\rangle\\ + B|a(\omega-\omega_M)\rangle + B^\dagger|a(\omega+\omega_M)\rangle\,,\end{aligned} \tag{4}$$

where $H_0 = \Omega_0 + i\Gamma$ and $B = \beta/2\begin{pmatrix}1 & 0\\ 0 & e^{i\phi}\end{pmatrix}$. The applied modulation converts the input signal up and down in frequency such that inputs with a single frequency will generate infinitely many sidebands equally separated by multiples of $\pm\omega_M$. These sidebands are coupled to each other through the B matrix. Thus, Eq. (4) is actually a set of infinitely many equations that can be written as [36]

$$\omega|\alpha(\omega)\rangle = \mathcal{H}|\alpha(\omega)\rangle + \mathcal{K}^T|\sigma_+(\omega)\rangle\,, \tag{5}$$

where $\mathcal{K}$ is a block-diagonal matrix where each block is K, and $\mathcal{H}$ is the block-tridiagonal matrix

$$\mathcal{H} = \begin{pmatrix}\ddots & \ddots & 0 & 0 & 0\\ \ddots & H_0-\omega_M I_2 & B & 0 & 0\\ 0 & B^\dagger & H_0 & B & 0\\ 0 & 0 & B^\dagger & H_0+\omega_M I_2 & \ddots\\ 0 & 0 & 0 & \ddots & \ddots\end{pmatrix}.$$

The amplitude vectors $|\alpha(\omega)\rangle$ and $|\sigma_\pm(\omega)\rangle$ are

$$|\alpha(\omega)\rangle = \begin{pmatrix}\vdots\\ |a(\omega+\omega_M)\rangle\\ |a(\omega)\rangle\\ |a(\omega-\omega_M)\rangle\\ \vdots\end{pmatrix},\ |\sigma_\pm(\omega)\rangle = \begin{pmatrix}\vdots\\ |s_\pm(\omega+\omega_M)\rangle\\ |s_\pm(\omega)\rangle\\ |s_\pm(\omega-\omega_M)\rangle\\ \vdots\end{pmatrix}.$$

The output of the system $|\sigma_-(\omega)\rangle$ can be found through

the expression

$$|\sigma_-(\omega)\rangle = |\sigma_+(\omega)\rangle + i\mathcal{K}\,|\alpha(\omega)\rangle\,. \tag{6}$$

The relation between the input and output of the system is given by the expression $|\sigma_-(\omega)\rangle = \mathcal{S}(\omega)\,|\sigma_+(\omega)\rangle$, where the full scattering matrix $\mathcal{S}(\omega)$ can be found by solving Eqs. (5) and (6). However, the linear scattering matrix $S(\omega)$ which only relates inputs and outputs at the same frequency and satisfies $|s_-(\omega)\rangle = S(\omega)\,|s_+(\omega)\rangle$ is typically more useful, especially if the input is monochromatic $|\sigma_+(\omega)\rangle = |s_+(\omega)\rangle$. This simpler scattering matrix can be found by using perturbation theory that ignores sideband terms beyond a certain order in the squared modulation amplitude β^2. In order for a system to be nonreciprocal, or different under an exchange of inputs and outputs, the scattering matrix must be asymmetric ($S(\omega) \neq S^T(\omega)$). In the following analysis, we aim to illustrate the origin of the linear nonreciprocal effect and therefore solve for $S(\omega)$ by keeping only the first-order sidebands (perturbation order β^2) [37] and neglecting the coupling between the sidebands and the ports.

The complex transmission function of the unmodulated two-resonator chain described by H_0, which can be found by solving Eqs. (2) and (3) with $\Omega_1 = 0$, is

$$\tau(\omega) = \frac{k^2\lambda}{[\gamma + i(\omega-\omega_0)]^2 + \lambda^2}. \tag{7}$$

The transmission amplitude and phase, shown in Fig. 1b, are respectively symmetric and anti-symmetric about the center frequency ω_0. As we will later show, the anti-symmetry of the phase response is vital to breaking reciprocity. There are two peaks in the transmission amplitude, corresponding to the eigenmode frequencies $\omega_0 \pm \lambda$. Near these resonant frequencies, the transmission phase is $\approx \mp\pi/2$ relative to the transmission phase at ω_0.

The modulated chain can be interpreted as a time-invariant 2D array with a synthetic dimension arising in frequency space. This array consists of the original chain and two additional chains for each perturbation order (one additional chain for each sideband). To first order, the system consists of three unmodulated two-resonator chains separated in frequency, as shown in Fig. 1c. The coupling rate $\beta/2$ between neighboring chains/sidebands is determined by the amplitude of the applied modulation. We can capture the effects of the modulation frequency and phase by introducing two synthetic fields - an electric field $\vec{\mathcal{E}}$ pointing parallel to the frequency axis, and a magnetic field $\vec{\mathcal{B}}$ pointing out of the 2D plane. The electric field manifests as a potential gradient of ω_M between the resonator chains, and is equivalent to the frequency offset of the H_0 matrix along the diagonal of $\mathcal{H}$. The magnetic field produces a magnetic flux that induces a direction-dependent phase shift of ϕ in each plaquette [12, 15], equivalent to the the phase term $e^{i\phi}$ in the B matrix. For simplicity, and because distance is not well defined in the synthetic dimension, we adopt units where $|\vec{\mathcal{E}}| = \omega_M$ and $|\vec{\mathcal{B}}| = \phi$.

Transmission through the system shown in Fig. 1c can be calculated as the sum of transmission through three channels: the central channel with no potential offset, the lower channel with a positive offset $+\omega_M$, and the upper channel with a negative offset $-\omega_M$. The lower and upper channels both enclose a synthetic magnetic flux which induces an additional direction-dependent phase shift of $\pm\phi$, such that the total transmission, written as a sum of symmetric and anti-symmetric parts, is

$$\begin{aligned} S_{21}(\omega) &\approx \tau + \frac{\beta^2}{4}\big([\tau_+ + \tau_-]\cos(\phi) - i[\tau_+ - \tau_-]\sin(\phi)\big), \\ S_{12}(\omega) &\approx \tau + \frac{\beta^2}{4}\big([\tau_+ + \tau_-]\cos(\phi) + i[\tau_+ - \tau_-]\sin(\phi)\big), \end{aligned} \tag{8}$$

where $\tau = \tau(\omega)$ and $\tau_\pm = \tau(\omega \pm \omega_M)$.

From Eq. (8), we find that the symmetric part of the transmission is identical between S_{21} and S_{12} (i.e., is reciprocal), while the anti-symmetric part differs (i.e., is nonreciprocal). It is immediately clear that if either synthetic field vanishes the system must be reciprocal, since $\sin(\phi = 0) = 0$ and $\tau_+ = \tau_-$ if $\omega_M = 0$. Furthermore, the strongest nonreciprocal response will arise when both ω_M and ϕ are tuned such that transmission is maximally anti-symmetric with respect to the sign of either quantity. This occurs when the input frequency $\omega = \omega_0$, the synthetic flux $\phi = \pm\pi/2$, and the synthetic potential $\omega_M \approx \lambda$, such that the lower and upper paths are resonant and respectively provide opposite $\pm\pi/2$ phase shifts due to the anti-symmetric phase of $\tau(\omega)$. The resonance of the lower and upper paths also maximizes the amplitudes of $\tau_\pm$ and therefore the β^2 term of Eq. (8), further increasing the nonreciprocal contrast.

The effect of the synthetic electric and magnetic fields can be interpreted as a Hall effect for photons. In the ordinary Hall effect, current flows perpendicular to applied electric and magnetic fields because the combination of fields exerts a force that makes it more favorable for electrons to move in one direction. Here, the same combination of fields makes it more favorable for photons to move in one direction, leading to transmission nonreciprocity. This effect is resonantly enhanced in our system, leading to a strong nonreciprocal contrast.

To test these predictions we implemented a chain of two coupled resonators with modulated resonance frequencies in a microwave circuit using microstrip stub resonators, as pictured in Fig. 2a (see Supplement S4 for additional details). Each resonator has an initial loaded resonance frequency $\omega_0/2\pi \approx 1.35$ GHz and is terminated in a varactor diode that modulates the resonance frequency in response to an applied voltage. We used external tunable phase shifters to control the phase shift

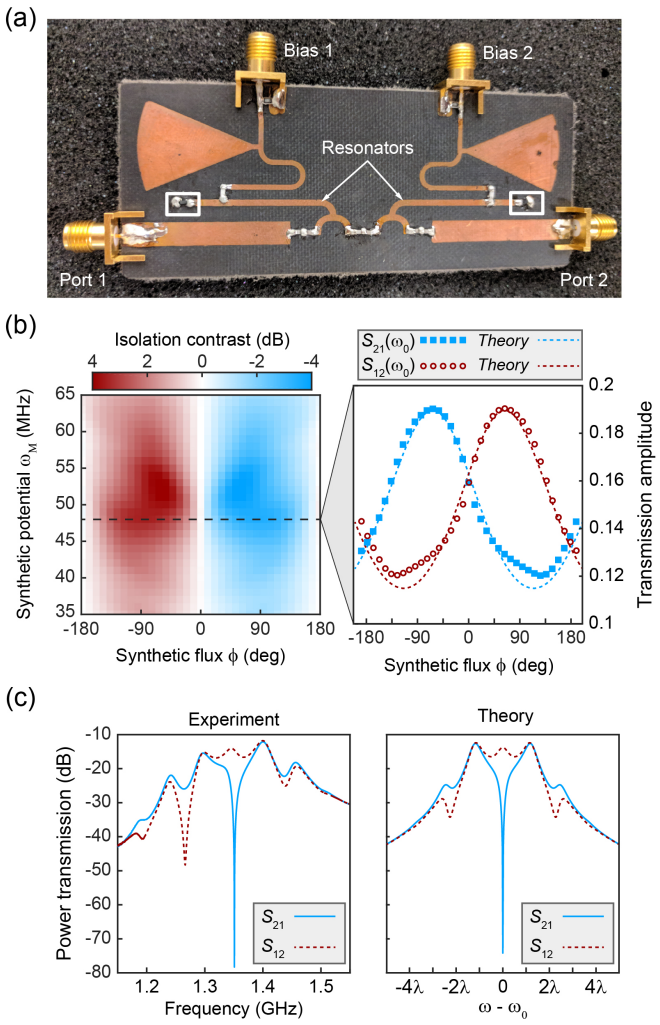

FIG. 2. (a) Photograph of the experimental circuit implementing two coupled resonators with variable resonance frequencies. The bias ports are used to apply a voltage to the varactor diodes (white boxes) and thereby modulate the resonant frequency. (b, left) Measured isolation contrast at ω_0 as a function of ω_M and ϕ. (b, right) Measured forward and backward transmission amplitude at $\omega_M/2\pi = 48$ MHz, which corresponds to the dashed line on the left. (c) Measured and fitted power transmission for the circuit in (a), with $\omega_M \approx \lambda$, $\phi = \pi/2$, and β tuned to minimize forward transmission amplitude.

ϕ between the sinusoidal voltage biases applied to the resonators.

We first swept the amplitudes of the synthetic fields (by adjusting the modulation frequency and phase) to find the values that produce the strongest nonreciprocity. Fig. 2b shows the measured isolation contrast for an input frequency of ω_0 as a function of the synthetic potential $\omega_M \propto \vec{\mathcal{E}}$ and synthetic magnetic flux $\phi \propto \vec{\mathcal{B}}$. As predicted, the contrast is maximized near specific values of these parameters: $\omega_M/2\pi \approx \lambda/2\pi \approx 48$ MHz, and $\phi \approx \pi/2$. The frequency dependence of the circuit components produce an additional asymmetry, not accounted for in our model which has frequency-independent parameters, that shifts the maximum contrast to $\omega_M/2\pi = 53$ MHz. The measured transmission amplitude for an input at ω_0 is shown in Fig. 2b for $\omega_M/2\pi = 48$ MHz. There is good agreement between the measured transmission and theoretically calculated transmission. This experiment also clearly demonstrates that the synthetic electric and magnetic fields work together to produce a strong nonreciprocal response. The measured transmission with no synthetic flux ($\phi = 0$) is fully reciprocal, and the isolation contrast decreases as the synthetic potential moves away from $\omega_M \approx \lambda \approx 48$ MHz, as expected.

Next we increased the modulation amplitude to minimize the transmission amplitude in the forward direction ($S_{21} \approx 0$) while maximizing isolation contrast. Figure 2c shows the measured and calculated values of the power transmission, $|S_{12}(\omega)|^2$ and $|S_{21}(\omega)|^2$, under modulation with this critical amplitude. Here, the modulation frequency has been increased to $\omega_M/2\pi = 53$ MHz in order to maximize the contrast. The measured forward transmission approaches zero (≈ -79 dB) at ω_0 and measured isolation contrast at ω_0 is > 64 dB. The calculated transmission matches the measured data well and the result is consistent with the prediction of Eq. (8). We note that the spectral asymmetry in the experimental data is caused by the frequency dependent coupling rate of the capacitors, which is not included in the theoretical model.

The synthetic electric and magnetic field interpretation of a modulated resonator chain can be extended to chains of an arbitrary length. The form of $\mathcal{H}$ remains the same regardless of chain length, only the inner matrices H_0 and B change to accommodate more resonators. A detailed explanation of the coupled-mode theory for longer modulated chains is provided in the Supplement S1.

Since all resonator chains have an anti-symmetric phase response about their center frequency, a combination of synthetic electric and magnetic fields can break reciprocity in a chain of any length through the nonreciprocal mechanism that we have identified. The outermost eigenmodes of resonator chains always follow the pattern found in the two-resonator chain: the phase difference between adjacent resonators, relative to the phase difference at ω_0, is $+\pi/2$ for the lowest-frequency mode and $-\pi/2$ for the highest mode. Strong transmission nonreciprocity will occur for inputs at the center frequency ω_0 when the synthetic flux $\phi = \pi/2$ and the synthetic potential $\omega_M = \Delta\omega$, where $\Delta\omega$ is the frequency separation between the outermost eigenmodes and the center frequency. In the shortest case of two resonators $\Delta\omega = \lambda$, but as the chain length increases $\Delta\omega \to 2\lambda$. A theoretical analysis of how this mechanism works in a three-resonator chain is provided in the Supplement S2.

We implemented a longer chain of three modulated res-

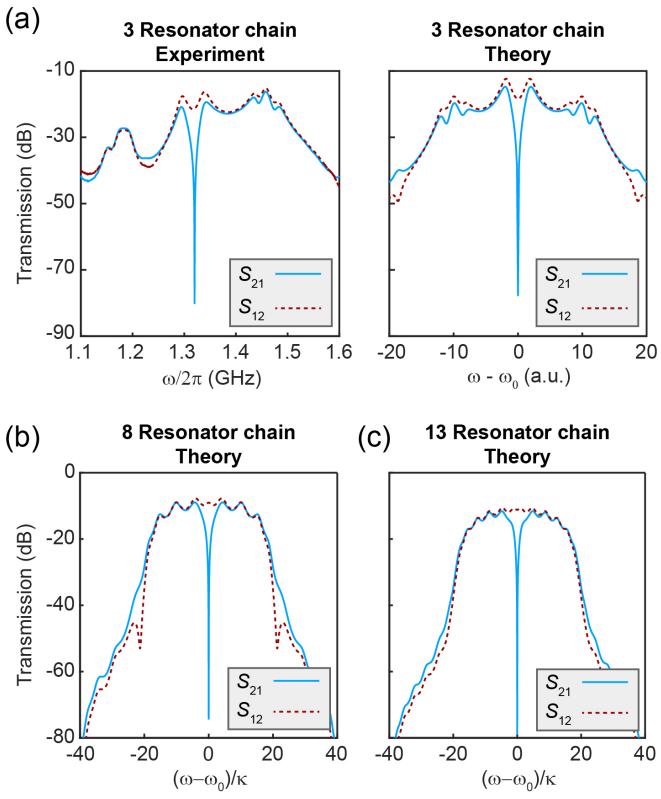

FIG. 3. (a) Measured and fitted power transmission for the three-resonator chain, with $\omega_M = \Delta\omega$, $\phi = \pi/2$, and β tuned to minimize forward transmission amplitude. (b) Calculated transmission for an 8 resonator chain under modulation with $\omega_M = \Delta\omega$, $\phi = \pi/2$, and β tuned to minimize forward transmission amplitude. (c) Calculated transmission for a 13 resonator chain under modulation with $\omega_M = \Delta\omega$, $\phi = \pi/2$, and β tuned to minimize forward transmission amplitude.

onators using three microstrip resonators with voltage-controlled resonance frequencies (photo in Supplement S2). Here, each resonator has an initial loaded resonance frequency $\omega_0 \approx 1.32$ GHz. The measured and calculated transmission spectra are shown in Fig. 3a for $\phi = \pi/2$ and $\omega_M/2\pi = \Delta\omega/2\pi \approx 141$ MHz, where the modulation amplitude is tuned to minimize the forward transmission amplitude. As in the two-resonator chain, the measured forward transmission near ω_0 approaches zero (≈ -80 dB), and there is strong nonreciprocal contrast (≈ 59 dB).

We also simulated longer chains using the coupled-mode theory model with intrinsic resonator linewidth κ, $\lambda = 10\kappa$, $k = 2\sqrt{\kappa}$, $\phi = \pi/2$, and keeping sideband terms up to $\pm 5\omega_M$. As the chain length increases, the number of eigenmodes of the chain increases proportionally, eventually forming a flat passband around ω_0 as the modes overlap due to their finite linewidth. Additionally, the backward transmission (insertion loss) approaches the reciprocal transmission of an unmodulated resonator chain (see Supplement S3B for more detail on insertion loss). We plot the forward (S_{21}) and backward (S_{12}) transmission spectra for chains of 8 and 13 resonators under modulation with $\phi = \pi/2$, $\omega_M = \Delta\omega$, and β tuned to minimize $S_{21}(\omega_0)$ in Fig. 3b,c. Despite the increased number of eigenmodes forming a passband instead of discrete resonances, the major nonreciprocal feature remains the large nonreciprocal dip near ω_0. The spectrum is approximately reciprocal between the central frequency and the band edges, indicating that the main nonreciprocal mechanism is the first-order process related to the anti-symmetric eigenmodes. Accordingly, the bandwidth of the nonreciprocity is primarily determined by the linewidth of these two modes. However, we note that the bandwidth is also influenced by the modulation frequency, amplitude, and phase, such that no simple expression relates it to the mode linewidth (see Supplement S3A for more detail).

The synthetic field interpretation of spatiotemporal modulation discussed here can be directly applied to a wide variety of nonreciprocal systems [9, 11–15, 20]. Additionally, the nonreciprocal mechanism we proposed is general and can be realized without added filters in any system of coupled resonators with the appropriate anti-symmetric modes, including chains of coupled photonic or electronic crystal defects. Since resonance frequency modulation is practical across a variety of resonator types [14, 38–40], the proposed method for generating strong nonreciprocity can be implemented across domains, in optical, microwave, or mechanical resonators. Furthermore, analogous modulation schemes that make use of both the lower and upper sidebands could also be realized using other methods of modulation, such as with Josephson parametric converters [8, 41, 42].

ACKNOWLEDGEMENTS

We thank Prof. Jennifer T. Bernhard for access to the resources at the UIUC Electromagnetics Laboratory. This project was supported by the US National Science Foundation (NSF) grants EFMA-1627184 (EFRI) and DMR-1351895, the US Office of Naval Research Director for Research Early Career Grant, and an NSF Graduate Research Fellowship for CWP.

[1] J. W. Strutt, Proceedings of the London Mathematical Society **4**, 357 (1873).
[2] J. R. Carson, The Bell System Technical Journal **3**, 393 (1924).
[3] D. Jalas, A. Petrox, M. Eich, W. Freude, S. Fan, Z. Yu, R. Baets, M. Popovic, A. Melloni, J. D. Joannopoulos, M. Vanwolleghem, C. R. Doerr, and H. Renner, Nature Photonics **7**, 579 (2013).

[4] C. L. Hogan, The Bell System Technical Journal **31**, 1 (1952).
[5] H. B. G. Casimir, Proceedings of the IEEE **51**, 1570 (1963).
[6] N. A. Estep, D. L. Sounas, and A. Al, IEEE Transactions on Microwave Theory and Techniques **64**, 502 (2016).
[7] B. Lax and K. J. Button, *Microwave Ferrites and Ferrimagnetics* (McGraw-Hill, 1962).
[8] A. Kamal, J. Clarke, and M. H. Devoret, Nature Physics **7**, 311 (2011).
[9] Z. Yu and S. Fan, Nature Photonics **3**, 91 (2008).
[10] M. Hafezi and P. Rabl, Optics Express **20**, 7672 (2012).
[11] H. Lira, Z. Yu, S. Fan, and M. Lipson, Physical Review Letters **109**, 033901 (2012).
[12] K. Fang, Z. Yu, and S. Fan, Physical Review Letters **108**, 153901 (2012).
[13] K. Fang, Z. Yu, and S. Fan, Physical Review B **87**, 060301 (2013).
[14] N. A. Estep, D. L. Sounas, J. Soric, and A. Al, Nature Physics **10**, 923 (2014).
[15] L. D. Tzuang, K. Fang, P. Nussenzveig, S. Fan, and M. Lipson, Nature Photonics **8**, 701 (2014).
[16] S. Qin, Q. Xu, and Y. E. Wang, IEEE Transactions on Microwave Theory and Techniques **62**, 2260 (2014).
[17] J. Kim, M. C. Kuzyk, K. Han, H. Wang, and G. Bahl, Nature Physics **11**, 275 (2015).
[18] N. Chamanara, S. Taravati, Z.-L. Deck-Leger, and C. Caloz, Physical Review B **96**, 155409 (2017).
[19] D. B. Sohn, S. Kim, and G. Bahl, Nat. Photon. **12**, 91 (2018).
[20] C. W. Peterson, S. Kim, J. T. Bernhard, and G. Bahl, Science Advances **4**, eaat0232 (2018).
[21] N. Bernier, L. Toth, A. Koottandavida, M. A. Ioannou, D. Malz, A. Nunnenkamp, A. Feofanov, and T. Kippenberg, Nature Communications **8**, 604 (2017).
[22] G. A. Peterson, F. Lecocq, K. Cicak, R. W. Simmonds, J. Aumentado, and J. D. Teufel, Phys. Rev. X **7**, 031001 (2017).
[23] B. Abdo, K. Sliwa, L. Frunzio, and M. Devoret, Physical Review X **3**, 031001 (2013).
[24] B. Abdo, K. Sliwa, S. Shankar, M. Hatridge, L. Frunzio, R. Schoelkopf, and M. Devoret, Phys. Rev. Lett. **112**, 167701 (2014).
[25] C. Macklin, K. O'Brien, D. Hover, M. E. Schwartz, V. Bolkhovsky, X. Zhang, W. D. Oliver, and I. Siddiqi, Science **250**, 307 (2015).
[26] L. Yuan, Q. Lin, M. Xiao, and S. Fan, Optica **5**, 1396 (2018).
[27] R. O. Umucalılar and I. Carusotto, Phys. Rev. A **84**, 043804 (2011).
[28] L. Yuan, Y. Shi, and S. Fan, Optics Letters **41**, 741 (2016).
[29] T. Ozawa, H. M. Price, N. Goldman, O. Zilberberg, and I. Carusotto, Phys. Rev. A **93**, 043827 (2016).
[30] S. Walter and F. Marquardt, New Journal of Physics **18**, 113029 (2016).
[31] L. Yuan and S. Fan, Optica **3**, 1014 (2016).
[32] Q. Lin, M. Xiao, L. Yuan, and S. Fan, Nature Communications **7**, 13731 (2016).
[33] X.-F. Zhou, X.-W. Luo, S. Wang, G.-C. Guo, X. Zhou, H. Pu, and Z.-W. Zhou, Phys. Rev. Lett. **118**, 083603 (2017).
[34] E. H. Hall, American Journal of Mathematics **2**, 287 (1879).
[35] W. Suh, Z. Wang, and S. Fan, IEEE Journal of Quantum Electronics **40**, 1511 (2004).
[36] J. H. Shirley, Phys. Rev. **138**, B979 (1965).
[37] We keep terms up to the fifth order ($\pm 5\omega_M$) in all theoretical calculations in this paper. See Supplement S1, which includes Ref. [43], for details on the calculation of the scattering matrix.
[38] Q. Xu, B. Schmidt, S. Pradhan, and M. Lipson, Nature **435**, 325 (2005).
[39] G. T. Reed, G. Mashanovich, F. Y. Gardes, and D. J. Thomson, Nature Photonics **4**, 518 (2010).
[40] M. M. Torunbalci, T. J. Odelberg, S. Sridaran, R. C. Ruby, and S. A. Bhave, IEEE Microwave and Wireless Components Letters (2018).
[41] N. Bergeal, R. Vijay, V. E. Manucharyan, I. Siddiqi, R. J. Schoelkopf, S. M. Girvin, and M. H. Devoret, Nature Physics **6**, 296 (2010).
[42] N. Bergeal, F. Schackert, M. Metcalfe, R. Vijay, V. E. Manucharyan, L. Frunzio, D. E. Prober, R. J. Schoelkopf, S. M. Girvin, and M. H. Devoret, Nature **465**, 64 (2010).
[43] K. Bowden, International Journal of General Systems **15**, 185 (1989).